Article

Impact of Cholesterol Concentration and Lipid Phase on Structure and Fluctuation of Amyloid Precursor Protein

Published as part of The Journal of Physical Chemistry virtual special issue "Ruth Nussinov Festschrift".

George A. Pantelopulos, Afra Panahi, and John E. Straub*

Read Online

ACCESS | Metrics & More | Article Recommendations | Supporting Information

ABSTRACT: Elevated levels of cellular cholesterol have been identified as one factor contributing to the onset of Alzheimer's disease (AD). Specific interaction between cholesterol and the amyloid precursor protein (APP), investigated via NMR experiments and computational studies, has been proposed to play a critical role in the processing of APP by secretases and the biogenesis of amyloid-β (Aβ) protein. We present all-atom molecular dynamics simulations of the 40-residue congener of the C-terminal domain of APP, C99$_{16-55}$ (C99), in cholesterol-enriched DMPC lipid bilayers. We investigated the effect of cholesterol concentration on the conformational ensemble of wild-type C99 and C99−cholesterol associations at the low pH of endosomal environments, at which residues E22 and D23 are neutral. C99 was also characterized in liquid ordered domains for Dutch (E22Q) and Iowa (D23N) Familial AD mutants at low pH and for the wild-type sequence using protonation states characteristic of neutral pH. Our results reproduce the equilibrium constant of past NMR characterizations of the C99−cholesterol interaction but are not consistent with the C99−cholesterol binding hypothesis. We find that the lifetimes of both DMPC and cholesterol complexed with C99 display a power-law distribution of residence lifetimes. Longer-lived C99−DMPC and C99−cholesterol complexes are primarily stabilized by salt bridges and hydrogen bonds of lysine amines to phosphate and hydroxyl groups. Nevertheless, specific interfaces for C99−cholesterol association which are not present for DMPC can be identified. Changes to C99−cholesterol interfaces are found to depend on C99 tilt angle and orientation of the juxtamembrane domain of C99 containing residues E22 and D23. These observations support a more nuanced view of the C99−cholesterol interaction than has previously been suggested. We propose that cholesterol modulates the conformation and activity of C99 and other small transmembrane proteins indirectly through induction of the liquid ordered phase and directly through hydrogen bonding. This suggests a critical role for membrane heterogeneity introduced by cholesterol in modulating the structural ensemble of C99 and the production of Aβ.
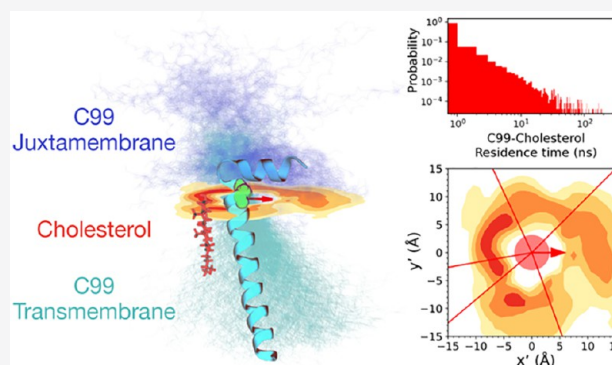
INTRODUCTION

The onset of Alzheimer's disease (AD) has long been correlated to enhanced levels of cholesterol resulting from diet, genetic predisposition, or aging.[1−8] Evidence suggests enhancement of cellular cholesterol concentration upregulates the amyloid cascade pathway,[3,9] in which amyloid precursor protein (APP) is processively cleaved by β- and γ-secretase to produce Aβ peptides of various lengths.[10−14] The Aβ_{42} and Aβ_{43} isoforms are of principal importance to the formation of Aβ oligomers and fibrils. Aggregates enriched in these isoforms are implicated with the onset of AD via the amyloid cascade hypothesis.[13]

β-Secretase is evidenced to cleave APP in the lipid rafts[9,15,16] of endosomes from the trans-Golgi network and the plasma membrane[17−19] to produce C99. γ-Secretase is also evidenced to reside in lipid rafts of these same cellular compartments where it processes C99 to form various isomers of Aβ.[9,15,16] As

such, lipid rafts are central to the production of both C99 from APP and Aβ from C99. Lipid rafts are domains in lipid membranes characterized by the liquid ordered (L$_o$) thermodynamic phase, which is more dense and ordered than the liquid disordered (L$_d$) phase that characterizes the bulk membrane.

Lipid raft domains are predominantly distinguished by their high but widely varying concentrations of cholesterol, sphingolipids, and gangliosides. However, the membrane L$_o$

phase itself can be most simply modeled as a binary mixture consisting of cholesterol and a lipid with two saturated tails. Within such binary lipid bilayers, the L_d to L_o phase transition occurs continuously as cholesterol concentration increases from 0 to 20 mol %.[20−24] When cellular cholesterol levels are low, lipid rafts cannot form APP−β-secretase associations supported by lipid rafts. Instead, APP preferentially associates with and is processed by α-secretase, producing the non-amyloidogenic C83, ending the amyloid cascade.[25]

In addition to cholesterol's role in lipid raft formation, cholesterol has been proposed to modulate C99 conformation through a C99−cholesterol complex. The C99−cholesterol complex was first suggested by Sanders and co-workers based on observations of shifts in the ^{1}H−^{15}N 2D NMR spectra of C99 as a function of the concentration of cholesterol analogue β-CHOLBIMALT in LMPG micelles.[26,27] Subsequent experiments by Barrett et al.[28] in DMPC:DHPC bicelles led to the proposal that C99 binds to cholesterol (Chol) via the glycine-rich face of the N-terminal region of the transmembrane domain (TMD). The same glycine-rich face plays a role in stabilizing C99 homodimers.[29−31] It was further proposed that the binding site is completed by formation of a short reentrant juxtamembrane (JM) helix. Further studies by Song et al. characterized the equilibrium constant of C99−Chol association, $K_d^{C99−Chol}$, in POPC:POPG lipid vesicles as 2.7 ± 0.3 mol % ($−2.1$ kcal/mol) via fitting changes in chemical shift as a function of protein and cholesterol concentration to a phenomenological kinetic model.[32] The observed association is weaker than typical protein backbone−water hydrogen bonds (H-bonds).[33]

The TMD of C99 (G$_{29}$AIIGLMVGGVVIATVIVITL-VMLKKK$_{55}$) contains several sequence motifs known to stabilize canonical "GAS$_{right}$" homodimers, including G$_{29}$xxxG$_{33}$xxxG$_{37}$ (a glycine zipper) and G$_{38}$xxxA$_{42}$.[34−36] Sanders has proposed that the glycine zipper provides a "groove" that supports contacts between the C99 TMD and the smooth α-face of Chol.[27] All-atom MD simulations of the C99 TMD in DMPC:Chol bilayers, employing initial conditions in which the Chol α-face is in contact with the G$_{29}$xxxG$_{33}$ face of C99 (Figure 1A−C), estimated the C99−Chol binding energy to be $−2.6 \pm 0.4$ kcal/mol.[37] A subsequent simulation study observed the pK_a of E22 and E23 of the C99 JM domain (K$_{16}$LVFFAED$_{23}$), having pK_as of 7.4 ± 0.1 and 6.5 ± 0.1, must be protonated to stabilize the JM helix and Chol interactions.[38] The JM domain helix can be destabilized when both E22 and D23 are protonated (neutralized) at pH 7. As such, the structure and function of the JM helix are different at the cytosolic pH of 7 experienced in plasma membranes and the luminal pH of 4.5−6.5 in endosomal membranes.[39] E22 and D23 are also sites for Familial AD (FAD) mutations, including the Dutch (E22Q)[40] and Iowa (D23N)[41] mutants.

The potential interplay of C99 and cholesterol are often discussed in terms of a strong C99−Chol complex.[42] The concept of a bound C99−Chol complex is surprising, as there is no precedent for cholesterol binding to other single-pass transmembrane proteins. Protein−cholesterol binding interfaces have been defined for multipass proteins such as G-coupled protein receptors (GPCRs) and ion channels.[43−54] These transmembrane interfaces have been characterized in terms of Cholesterol Recognition/interaction Amino acid Consensus (CRAC) sequences.[55,56] CRAC domain sequences are (L/V)-X$_{1−5}$-Y-X$_{1−5}$-(K/R), in which X$_{1−5}$ are any apolar
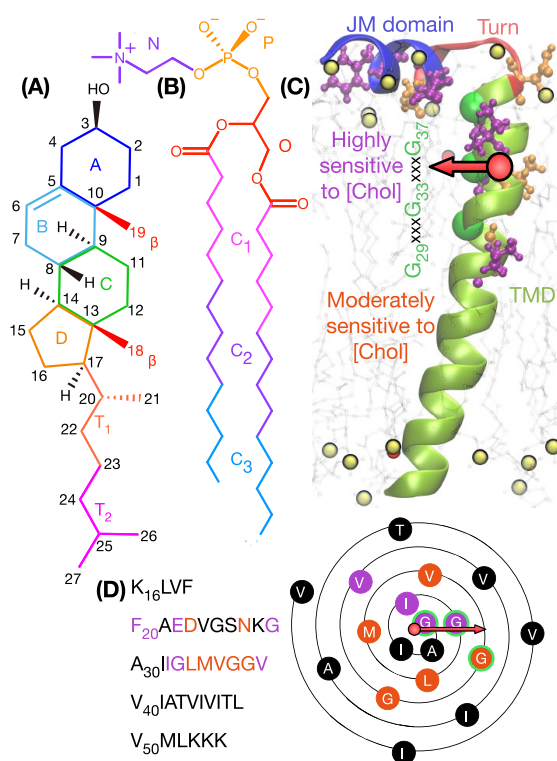
Figure 1. (A) Molecular structure of Chol, coloring the O, β, A-D rings, and T$_{1−2}$ groups used to average C99−Chol contacts. (B) Structure of DMPC, coloring the N, P, and C$_{1−3}$ groups used to average C99−DMPC contacts. (C) C99$_{16−55}$ of PDB 2LOH in a DMPC:Chol 8:2 membrane. JM domain, turn, and TMD labeled in blue, red, and green-yellow. Residues highly (moderately) sensitive to Chol concentration in purple (orange).[28] GxxxGxxxG motif Cα in green. DMPC (Chol) phosphorus (oxygen) in yellow (red) and lipid tails (transparent) within 10 Å shown for reference. C99$_{16−55}$ sequence displayed with residue coloring. (D) Wenxiang diagram of residues 29−46 of the transmembrane helix.

amino acid. CARC ("inverse" CRAC) domains are (K/R)-X$_{1−5}$-(Y/F)-X$_{1−5}$-(L/V).[57] Within these CRAC or CARC domains, the aromatic residues support Chol−protein π-stacking interactions with the Chol-α face assisted by van der Waals contacts with Leu or Val. These domains can also support H-bonding with Chol at the lipid−water interface with Arg or Lys. C99 contains one CARC sequence in the JM domain, K$_{16}$LVFFAEDV$_{24}$. Within this domain, the pH-switching residues E22 and D23 are present.

Barrett et al. studied C99 in DMPC:DHPC using ^{1}H−^{15}N NMR and observed chemical shifts that strongly (F$_{20}$, E$_{22}$, G$_{29}$, I$_{32}$, G$_{33}$, V$_{39}$) or moderately (D$_{23}$, N$_{27}$, L$_{34}$MVGG$_{38}$) respond to changes in Chol concentration.[28] It was suggested that these residues may constitute the binding interface (Figure 1C). However, the orientation of these residues around the helical TMD shows no particular face of C99 along which Chol would interact (Figure 1D). Taken together, these observations suggest that the C99−Chol complex is only moderately stable and may be less specific than previously proposed.

MD simulations have been used to explore protein−Chol binding interfaces in GPCRs employing the MARTINI lipid and protein model to explore possible protein−Chol complexes.[44−46,48−52] These coarse-grained simulations have led to the identification of contacts formed between multiple transmembrane helices. Putative protein−Chol binding com-

plexes are mapped to all-atom models to elucidate their structure and specific stabilizing interactions. Given the lack of significant structural pockets, this approach cannot be used to propose binding sites for Chol to single pass transmembrane proteins such as C99. In addition, coarse-grained models lack detailed H-bonding and π-stacking interactions necessary to support stable C99−Chol complexes,[58] making them unsuitable for the exploration of Chol−protein binding.

The minimal subsequence C99$_{16-55}$, K$_{16}$LVFFAED-VGSNKGAIIGLMVGGVVIATVIV-ITLVMLKKK$_{55}$, appears to be required to capture essential interactions between C99 and cholesterol. This congener contains the ubiquitous VGSN turn sequence, the central hydrophobic cluster KLVFFAED,[13,59] and the C99 TMD, including the K$_{53}$K$_{54}$K$_{55}$ lysine anchor.[30,60] For C99 in plasma membranes and micelles, experiment and simulation suggest that KLVFFAED will form a JM helix, that VGSNK forms a turn, and that GAIIGLMVGGVVIATVIVITLVMLKKK forms the α-helical C99 TMD.[26−28,58,60,61]

In this study, we employ unbiased MD simulations that make no prior assumption of the C99−Chol encounter complex to characterize the nature of the C99−Chol interaction in DMPC bilayers containing 0, 5, 10, and 20 mol % Chol. Four forms of C99 were studied, including (1) wild-type C99$_{16-55}$ neutral E22 and D23 or (2) charged E22 and D23, (3) the Dutch (E22Q)[40] with neutral D23 and Q23, and (4) Iowa (D23N)[41] mutant with neutral E22 and N23. We performed 70 unbiased, 1 μs all-atom simulations of C99$_{16-55}$.

Enhancements to cholesterol concentration, introducing the L$_o$ phase, change the structure of C99. We characterized the structure of C99 by TMD tilt, helical propensity, orientation of the JM domain, and height of the JM domain above the membrane surface. We also observed that the E22Q mutant, D23N mutant, and charge state of E22 and D23 in the L$_o$ phase also change the structure of C99. C99−cholesterol residence lifetimes were found to be power-law distributed with constants k in the range of 1.21−1.43, suggesting heterogeneity in the stability of C99−Chol complexes. Of these, long-lived C99−Chol complexes were found to be supported by hydrogen bonds of K16 and K28 with the Chol hydroxyl group in the upper leaflet (exo-facing in plasma membrane), and K53−K55 with the Chol hydroxyl group in the lower leaflet (cyto-facing in plasma membrane). Within the upper leaflet, it was found that the conformation of the JM domain creates unique interfaces for C99−Chol complexes whose potential of mean force is within 1 kcal/mol of the $K_d^{C99-Chol}$ determined by Song et al.[32] We conclude that monomeric C99 does not bind Chol through the formation of a specific, stable heterodimer. We find that multiple, specific C99−Chol complexes can form pending the conformational state of the C99 JM domain and lipid phase.

■ METHODOLOGY

Molecular Dynamics Simulation. The 40-residue C99$_{16-55}$ congener sequence was used to model C99. The CHARMM36 force field[62,63] was employed to describe the system by using ACE N-terminal and CT3 C-terminal capping groups. C99 was initiated from a configuration based on PDB 2LOH[64] in which the JM domain is structured and inserted into the membrane obtained from past simulation of wild-type C99 in DMPC:Chol 8:2 simulations.[38] Cholesterol was laterally distributed at random in the bilayer such that there was no C99−Chol dimer in the initial state. This is different

from past work exploring the C99−Chol complex, in which the initial state was a preformed C99−Chol complex at the GxxxG interface.[37,38] Lipid bilayers, each encapsulating the transmembrane domain of C99, were prepared in CHARMM by using the CHARMM-GUI system building protocol.[65−69]

The bilayer leaflets were constructed with an asymmetric number of lipids to support the insertion of the JM domain to the upper leaflet of the lipid bilayer. For 0, 5, 10, and 20 mol % systems 69, 66, 62, and 55 DMPC were used in the upper leaflet and 73, 69, 65, and 58 DMPC were used in the lower leaflet. For 5, 10, and 20 mol % systems, 3, 7, and 14 Chol were used in the upper leaflet and 4, 8, and 15 Chol were used in the lower leaflet. Approximately 46 waters per lipid and 17 Na$^+$ and Cl$^−$ ions (with additional counterions depending on the system) were used to solvate each lipid bilayer. Four different C99 proteins were simulated, including (1) at an effectively acidic pH, in which E22 and D23 were neutral (E22,D23[0]),[38] (2) at neutral pH (E22,D23[−]), and the (3) Dutch (E22Q[0]) and (4) Iowa (D23N[0]) FAD mutants at acidic pH. These acidic and neutral pH protonation states are representative of the endosomal and plasma membrane environments, respectively. Ten replicates of each of these proteins were prepared with unique, randomized lateral distributions of DMPC and Chol. Each system was minimized and then equilibrated using a processive release of restraints and associated increase from 1 to 2 fs integration time step as suggested by Wu et al.[68]

All molecular dynamics simulations were performed by using 25 2.4 GHz Intel Xeon E5-2680v4 CPUs and a P100 GPU using GROMACS 2018.3[70] at mixed precision to achieve a 86 ns/day rate of sampling for these ∼35900-atom simulations. The leapfrog integrator was used at a 2 fs time step in combination with hydrogen bond constraints via the SETTLE method.[71] Neighbor lists were updated every 20 steps by using the buffered Verlet neighbor scheme. Short-range interactions employed a 1.2 nm distance cutoff with a force switching function applied from 1.0 to 1.2 nm for Lennard-Jones and from 0 to 1.2 nm for electrostatic interactions. Long-range interactions were handled by using particle mesh Ewald[72] with a 0.12 nm grid spacing and fourth-order grid interpolation. A Nosé−Hoover thermostat[73] with one thermostatting chain and a time constant of 1 ps was used to control temperature to 310 K, separating C99, the lipid bilayer, and the solvent to three separate thermostat groups. The Parrinello−Rahman barostat[74] was used with the z-axis decoupled from the xy-plane employing a 5 ps time constant, a reference pressure of 1 bar, and a compressibility of 4.5×10^{-5} bar^{-1}. Each system was run for 1 μs of MD, summing to 70 μs of sampling. Coordinates were saved every 100 ps. All analyses employed this frame resolution, including 100000 frames in the analysis of each system.

Protein Conformational Analysis. Various descriptions of the protein conformational ensemble were employed to characterize essential changes to C99 structure in these different conditions. To describe insertion of the JM domain to (or evacuation from) the membrane surface, we evaluated the difference of the z-axial positions of K16 Cα atoms from the mean z-axial positions of the phosphorus of DMPC within the upper leaflet of each frame. The tilt (polar) angle (θ) of the protein TMD was determined from the angle between a vector that best fit the heavy backbone atoms of C99 in residues 30−55 and the bulk membrane normal (the z-axis) (Figure 2A). To describe the relative orientation of the JM domain to the
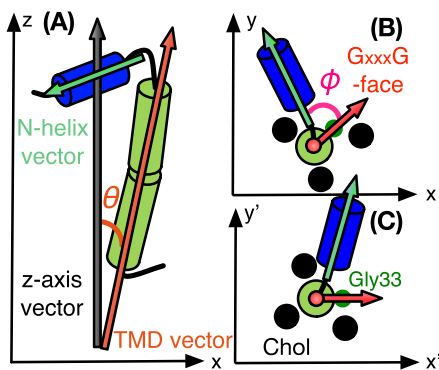
Figure 2. Cartoon representations of (A) TMD tilt angle (θ), (B) angle defining relative orientation of the JM domain and GxxxG director vector (ϕ), and (C) rotation about z-axis to align GxxxG director vector along the x'-axis.

GxxxG face, an azimuthal angle (ϕ) in the xy-plane was defined over 360°, in which 0° defines a perfect overlap of the JM domain and the GxxxG face. The director of the GxxxG face ($G_{29}AIIG_{33}LMVG_{37}$) was defined by taking the centroid of the xy-positions of residues 31−35 as the tail and the G33 Cα xy-position as the vector head. To define ϕ, a vector describing the JM domain was defined by determining a vector of best fit through heavy backbone atoms of residues 17−24 and enforcing the head to be at L_{17} and the tail to be at V_{24} (Figure 2B). To characterize the helicity of C99, H-bonds were identified between amide of each ith residue and any of the $i + 3$, $i + 4$, or $i + 5$ residue backbone oxygen atoms and counted toward a helix if present, with a 2.5 Å H−O distance criterion.

Protein−Cholesterol and Protein−DMPC Contact and Binding. To define the xy-plane distribution of upper-leaflet Chol or DMPC complexed with C99 relative to the GxxxG face, we rotated the coordinates of the system such that the xy-plane projection of the GxxxG face vector points along the positive x-axis, obtaining the position of solvating Chol or DMPC in these transformed x' and y' coordinates (Figure 2C). To determine contacts between C99 and Chol or DMPC, we used a 5 Å distance cutoff between heavy (non-hydrogen) atoms to define whether a contact was formed. To more easily represent C99−Chol contacts, contacts of each heavy atom on Chol (of 28) with each protein residue (of 40) were averaged over geometrically representative subunits of the Chol molecule, simplifying from 28 Chol contacts to 8. Subunits of Chol were assigned as O (O3) the oxygen headgroup, β (C18, C19) defining β-face methyl groups, the sterol rings A (C3, C2, C4, C1, C5, C6), B (C6, C10, C7, C9, C8), C (C9, C8, C11, C14, C12, C13), and D (C14, C13, C15, C16, C17), and the upper and lower segments of the carbon tail, T_1 (C20, C21, C22, C23) and T_2 (C24, C25, C26, C27) (Figure 1A). Similarly, to easily represent C99−DMPC contacts, the 46 heavy atoms of DMPC are averaged over the geometrically representative subunits of DMPC, simplified from 46 to 5 contacts. Subunits of DMPC were assigned as N (C13, C14, C15, N, C12, C11), P (O12, O13, O14, P, O11, C1), C1 (C22, C23, C24, C25, C26, C32, C33, C34, C35, C36), C2 (C27, C28, C29, C210, C37, C38, C39, C310), and C3 (C211, C212, C213, C214, C311, C312, C313, C314) (Figure 1B).

We tracked the "residence time" over which each Chol or DMPC remained in contact with C99. A 25 ns cutoff in residence time was used to distinguish complexed and transient Chol or DMPC upon inspection of residence time

probability distributions (see the Results section). The number of Chol or DMPC simultaneously solvating C99 was determined by counting the number of intersecting residence times between solvating Chol or DMPC (with residence times >25 ns) per frame in each simulation. This was done by first determining the number of n-mers of the highest order, progressively evaluating lower order n-mers down to a dimer, and removing frames found to intersect with other frames when determining the number of each n-mer present in the trajectory. This ensured that a given frame of a solvating Chol or DMPC could not be counted as part of both a higher- and lower-order n-mer. This analysis was performed in the upper and lower leaflets to quantify the number of simultaneously populated solvation sites of the C99 congener.

The angular distribution of the Chol mass density around the GxxxG face supported the definition of five unique C99−Chol interfaces in the upper leaflet (see the Results section). We determined the relative population and C99−Chol contacts for these five interfaces, defined based on the angular position around the GxxxG face vector. The interfaces labeled from 1 to 5 were assigned for Chol centers of mass at positions between 290−45°, 45−115°, 115−190°, 190−220°, and 220−290° relative to the GxxxG face vector. The relative orientation of these interfaces corresponds to the relative positioning of residues that exhibited strong or moderate changes in chemical shift as measured in past NMR studies of C99 (Figure 1C) in DHPC:DMPC:Chol bicelles.[28]

We measured the hydrogen bonds formed for solvating C99 or DMPC involving Lys 16, 28, 53, 54, and 55. From Lys, the amide nitrogen, N, amido nitrogen, NZ, and, for Lys 55, the capping nitrogen, NT, serve as donors and the carbonyl O3 serves as an acceptor. From Chol, the hydroxyl group, H3 and O3, serves as donor and acceptor. From DMPC there are three groups of acceptors. From the phosphate there are O11, O12, O13, and O14. From the ester groups on the lipid tails there are O21 and O22 and O31 and O32. A hydrogen bond was defined if the H−O distance is under 2.5 Å and if the N−H−O angle is larger than 150°. The Lys−phosphate hydrogen bonds measured here are more appropriately described as a salt bridge due to its ionic character, and we refer to it as such in the article.

■ RESULTS AND DISCUSSION

All-atom MD simulations of C99$_{16−55}$ employing neutral and protonated E22 and D23 corresponding to pH ≤ 6.5[38] were performed at 0, 5, 10, and 20 mol % cholesterol (Chol) in DMPC lipid bilayers mimicking experiments of Song et al.[32] At 20 mol % Chol, simulations of C99$_{16−55}$ at acidic pH (C99[E22,D23[0]]) and neutral pH (C99[E22,D23[−]]) were performed, along with simulations of the Dutch (C99[E22Q[0]]) and Iowa (C99[D23N[0]]) FAD mutants at acidic pH. These acidic and neutral protonation states mimic the endosomal and plasma membrane environments in which C99 is processed by γ-secretase to form amyloid beta (Aβ).[17−19,39] Analysis of ten 1 μs replicates of each system was used to characterize the conformational ensembles of C99 and interfaces of long-lived C99−Chol complexes.

C99 Conformational Ensemble. *Orientation of C99 Domains Depends on Cholesterol Concentration.* At 0, 5, 10, and 20 mol % Chol, the bilayer is characterized as a miscible mixture of DMPC and Chol. To characterize the effect of varying Chol concentration and lipid ordering, we computed the C99 tilt angle (θ) distribution, the relative orientation of
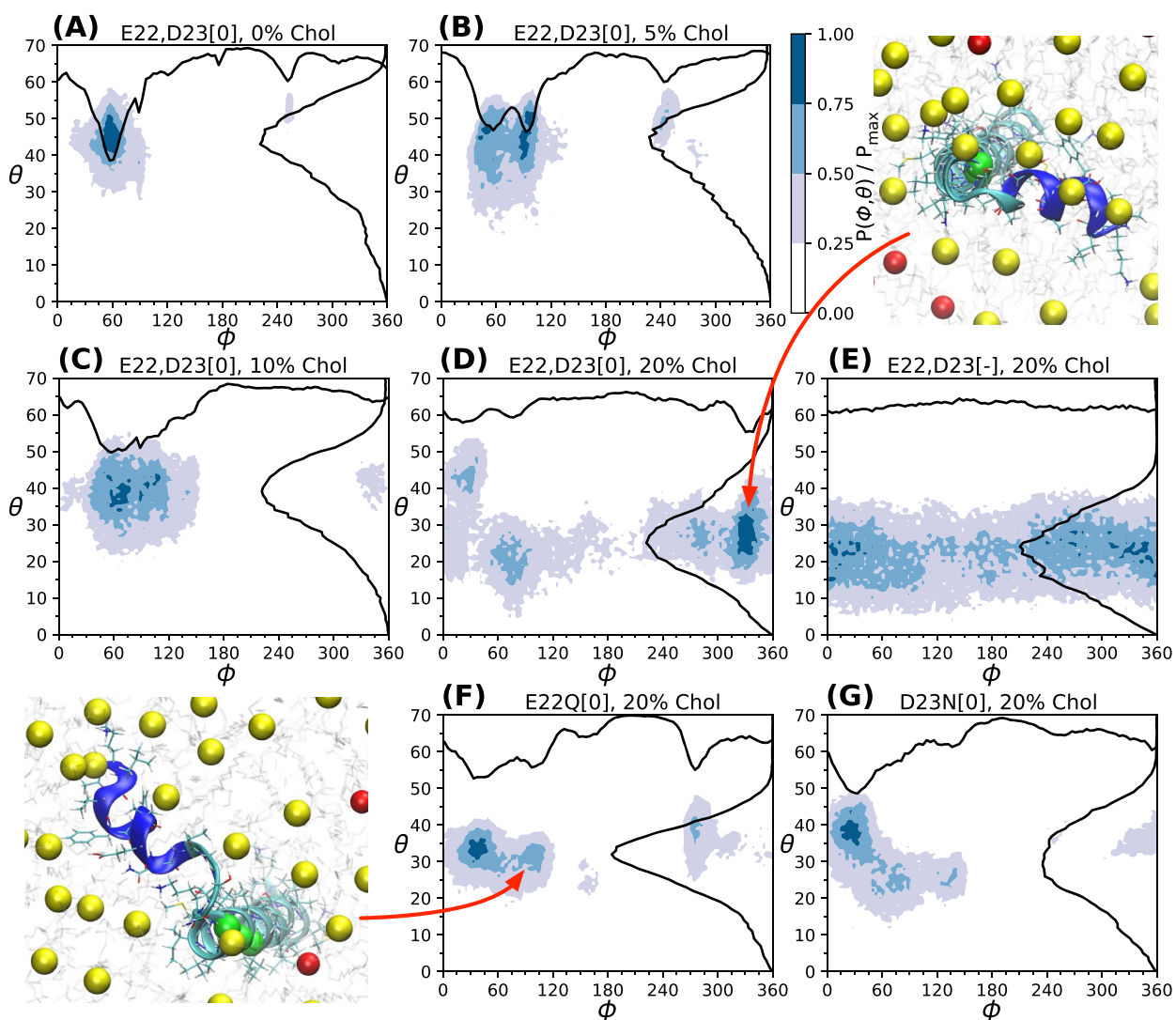
Figure 3. Scaled observations of C99 E22,D23N[0] TMD tilt angle (θ) and orientation of JM domain relative xy-plane orientation to the GxxxG face (ϕ) at (A) 0, (B) 5, (C), 10, and (D) 20 mol % Chol. (E) E22,D23N[−], (F) E22Q[0], and (G) D23N[0] distributions at 20 mol % Chol. Visualizations of the phosphorus and oxygen of DMPC and Chol (yellow and red) and C99 from above the xy-plane, coloring $G_{29,33,37}$ green and the JM domain blue.

the JM domain to the GxxxG face in the xy-plane (ϕ), the insertion depth of the JM domains to the membrane surface, and the helicity of C99 residues.

When the concentration of Chol is increased in saturated lipid bilayers, the L_o phase formed.[23] This manifests a commonly observed z-axial thickening and xy-plane condensation and ordering of lipids in the lipid bilayer that is expected to cause the C99 tilt angle (θ) to decrease. The C−H NMR order parameter was used to report on the enhancement in lipid tail ordering characteristic of the L_o phase, which we observe to be substantially enhanced by addition of Chol (Figure S1). What was not anticipated was the change in the xy-plane orientation of the JM domain relative to the GxxxG face in response to this ordering of the bilayer (ϕ). Analyses of the E22,D23[0] systems at 0, 5, and 10 mol % Chol exhibit θ distributions centered near 45° which shift to 25° in 20 mol % Chol, indicating a major change in TMD conformation in the L_o phase.

In ϕ, multiple states that do not interconvert are observed. The populations of these states at 20 mol % Chol are recorded

in Table S1. Typically, the JM domain positioned at $\phi = 60°$ or 340° counterclockwise from the GxxxG face are observed from the N-terminus, the latter becoming more populated at 20 mol % Chol (Figure 3A−D). However, the conformational distribution at 20 mol % Chol was found to be sensitive to both charge state and sequence of residues 22 and 23 (Figure 3D−G). For E22,D23[−], θ fluctuates about 20° and ϕ is random. E22Q[0] exhibits three clear states in ϕ, with the JM domain sitting at about $\phi = 60°$ and occasionally at $\phi = 280°$, and fluctuates about $\theta = 35°$. D23N exhibits slightly different behavior, as the JM domain populates three states characterized by $(\theta, \phi) = (40, 20°), (25, 60°)$, and $(25, 140°)$. These observed differences in JM domain orientation (ϕ) and TMD tilt angles (θ) appear to be signatures of where and how Chol interacts with C99. The observation that the conformational ensembles of the JM domain and TMD tilt depend sensitively on the chemical state suggests that these changes in charge state and sequence could impact C99 homodimerization and C99−γ-secretase binding.

Insertion of the JM Domain Depends on Sequence and Charge State. The insertion depth of K16 serves as a measure of JM domain orientation relative to the bilayer surface. For C99 E22,D23[0] we observe that insertion of the JM domain increases with increasing mol % Chol (Figure 4A). For
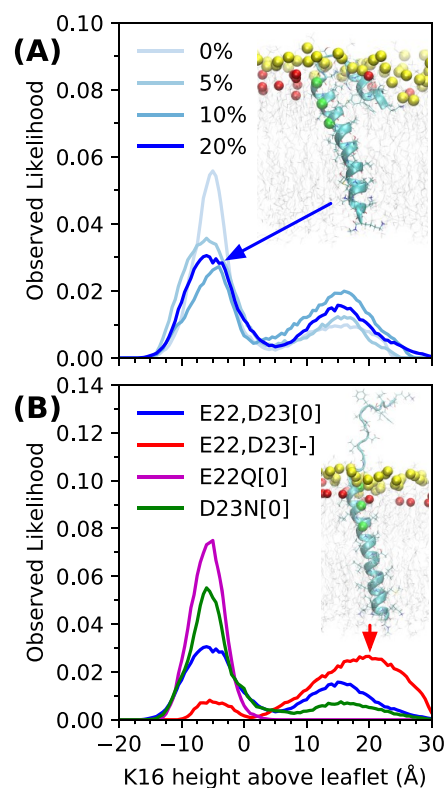
Figure 4. Probability densities of K16 height above mean DMPC phosphorus positions used to define the bilayer–solvent interface in upper leaflet (A) for E22,D23N[0] at varying mol % Chol and (B) at 20 mol % Chol. Insets depict phosphorus and oxygen of DMPC and Chol (yellow and red) and color $G_{29,33,37}$ green.

E22,D23[−] the JM domain is observed to rarely insert in the membrane surface (Figure 4B). It has been observed that insertion of the JM domain is necessary to complete the putative Chol binding site described by Sanders and co-workers, which involves hydrogen bonding of the JM domain to Chol O3.[38] In the FAD mutants, E22Q and D23N, insertion of the JM domain is observed to be enhanced. Notably, the JM domain of the E22Q[0] mutant is observed to be consistently inserted throughout the simulations.

JM Domain Structure Depends on pH. The presence of Chol in the membrane appears to shorten the α-helix of the C99 TMD of E22,D23[0] as the tilt angle of the TMD decreases (Figure 5A). The measured distribution is consistent with that observed for the full C99 sequence.[60] For E22Q[0] and D23N[0] we see similar helical propensities at 20 mol % Chol. However, in E22,D23[−] the JM domain is observed to be unstructured (Figure 5B). As observed previously, the charge state of E22 and D23 at neutral pH destabilizes the JM domain, leading to extension of the unstructured JM domain into solvent. This pH switch[38] supports a mechanism of pH-dependent insertion and evacuation of the JM domain in wild-type C99. However, this facility seems lost in the E22Q (Dutch) and D23N (Iowa) FAD mutants.
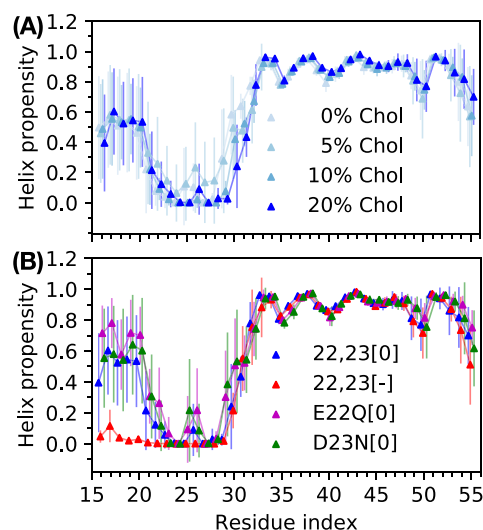

Figure 5. α-Helix propensity defined by likelihood of any backbone H-bond between each ith and $i \pm 3$, $i \pm 4$, or $i \pm 5$ residues at (A) for E22,D23N[0] and (B) at 20 mol % Chol averaged over replicate trajectories with corresponding standard deviations.

C99 Solvation by Cholesterol and DMPC. *Residence Times Suggest C99 Solvation but Not Binding.* The conjecture that cholesterol modulates the amyloid pathway by forming stable and specific complexes with C99 suggests that we should observe a relatively long-lived C99–cholesterol complex.[27] Within an ensemble of C99–Chol interactions, it should be possible to distinguish "bound" Chol from "unbound" Chol, the latter only forming transient contacts with lifetimes similar to those of other C99–lipid interactions, and that persist for lifetimes in excess of other Chol–lipid interactions (roughly ∼0.35 ns on average.)[75] To do this we observed the residence time for each observed C99–Chol and C99–DMPC contact pair, tracked for each 100 ps time frame, to identify any Chol or DMPC initially in contact with C99 that maintained any contact with C99. This analysis was performed for all C99–Chol and C99–DMPC contact pairs observed in each system. It was found that the average C99–Chol and C99–DMPC lifetime is approximately 1 ns, longer than that of lipid–lipid interactions (Table S2). The log−log likelihood distributions of C99–Chol and C99–DMPC residence are well described by a power law (Figure 6 and Figure S2). We find that the power law exponents, k, are similar for Chol and DMPC and are between 1.25 and 1.43. This suggests that the C99–Chol interaction observed in simulation and experiment is heterogeneous without a characteristic time or energy scale for binding. For this reason, we refer to Chol and DMPC that persist in contact with C99 for over 25 ns as solvating as opposed to bound.

C99–Cholesterol Aggregate Likelihood Distributions. Our results suggest Chol does not form stable and specific bound complexes with C99. To explore the nature of longer-lived associations having residence times >25 ns, we address the following questions. We address the following questions. How many Chol can concurrently solvate C99? Do C99–Chol complexes in one leaflet impact the formation of C99–Chol complexes in the opposite leaflet?

At 20 mol % we observe that Chol in the upper leaflet dimerizes with C99 between 20 and 40% of the time. Higher-order aggregates form with varying probability depending on
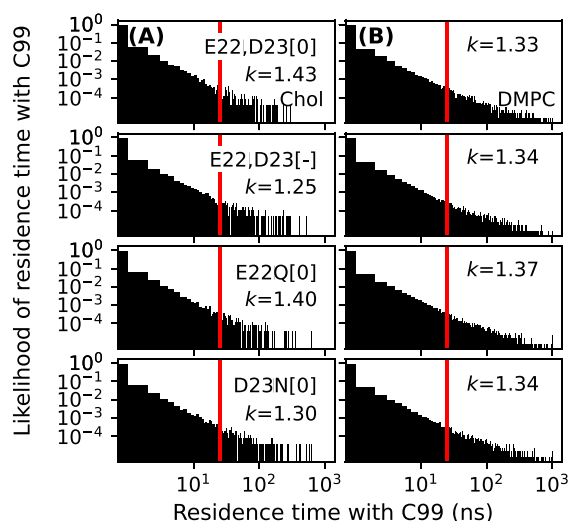
Figure 6. C99−Chol dimer residence times observed for all C99−Chol contact pairs at 20 mol % Chol. The red line indicates the 25 ns cutoff used to distinguish transient and complexed C99−Chol pairs. The inset notes power law exponents for C99−Chol residence times.

the state of residues 22 and 23 (Figure 7A). In C99 D23N[0], the C99−Chol dimer is as likely as Chol-free C99. In addition,
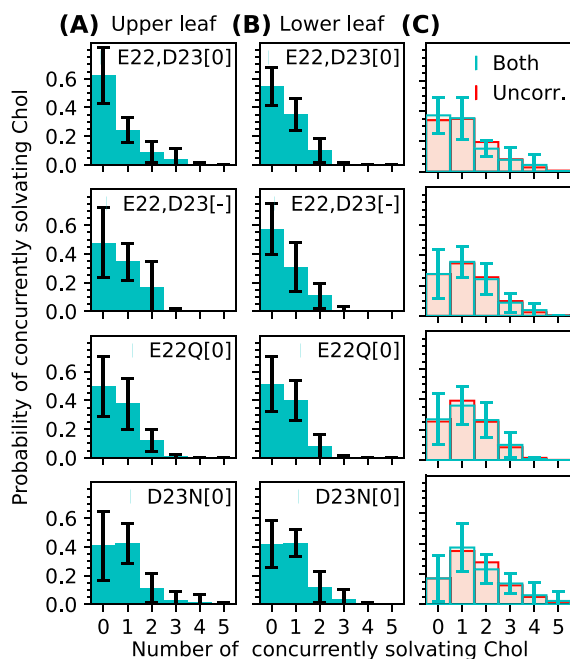
Figure 7. Observed probability densities of bound C99−Chol complexes in the upper (A) and lower (B) leaflets at 20 mol % Chol as well as (C) both leaflets (cyan) and the expectation for both leaflets assuming upper and lower leaflet distributions are uncorrelated (red). Averages and standard deviations are computed over 10 replicate trajectories.

the rare tetramer forms, suggesting that the conformational ensemble of the JM domain in D23N provides more unique and stable interfaces on C99 for solvation by Chol. In the lower leaflet, we see that E22,D23[0], E22,D23[−], and E22Q[0] exhibit similar C99−Chol aggregate likelihoods (Figure 7B). Here, too, D23N[0] exhibits enhanced C99−Chol aggregate likelihoods and sizes. As a function of Chol

concentration, the C99−Chol dimer is not observed in upper and lower leaflets of <10 mol % Chol in E22,D23[0] (Figure S3). By examining the solvating Chol oligomer distribution without discrimination between the upper and lower leaflet, compared with the joint probability distribution implied if distributions of the upper and lower leaflet are uncorrelated, we find that the oligomer distributions in the upper and lower leaflets are uncorrelated (Figure 7C). These observations imply that C99−Chol complexes are dependent on the conformational ensemble of C99, which is affected by the state of residues 22 and 23 and the introduction of the L_o phase by Chol.

Cholesterol Distribution about C99 TMD Assumes Multiple Complex Interfaces. As the JM domain assumes various orientations relative to the GxxxG face dependent on the charge state or sequence of C99 (see Figure 3), the solvation interfaces of C99−Chol in the upper leaflet are expected to display varying likelihoods and solvation motifs.

In the C99$_{16-55}$ congener, which lacks the C-terminal JM helix, the lower leaflet has no JM domain to obstruct Chol interactions with C99.[60] We characterized the *xy*-plane mass density of upper leaflet Chol about the C99 TMD with the director oriented outward from the GxxxG face (see Figure 8). This GxxxG face has previously been hypothesized to serve as a specific Chol binding site and serves as a primary binding interface for the C99 homodimer. The GxxxG face was defined in terms of a vector in the *xy*-plane fit through the center of geometry of IIG$_{33}$LM and the Cα of G33. We aligned the GxxxG face vector along the positive *x*-axis (now described using transformed coordinates *x′* and *y′*) and identified five unique faces of C99 that support C99−Chol solvation for varying chemical states of E22 and D23 at 20 mol % Chol (Figure 8). These five interfaces (labeled from 1 to 5) correspond to polar angles 290−45°, 45−115°, 115−190°, 190−220°, and 220−290°, respectively, relative to the GxxxG face vector (0°). The potential of mean force (PMF) of the masses of solvating Chol at these interfaces is between 2.5 and 3 kcal/mol, within 1 kcal/mol of of the $K_d^{C99-Chol}$ determined by Song et al.,[32] suggesting that these solvating Chol are a reasonable representation of the bound cholesterol proposed by Sanders and co-workers.

C99-Chol Complex Motifs Depend on Juxtamembrane Charge State and Sequence. C99−Chol contacts formed in the upper leaflet of each solvation interface around the GxxxG face were measured by using a 5 Å heavy atom distance contact criterion. Groups of averaged heavy atom contact pairs on Chol were used to define sites of interaction with C99 from the oxygen head (O), *β*-face (*β*), sterol rings A−D (A, B, C, D), and carbon tail segments (T$_1$, T$_2$) (see the Methodology section). C99−Chol contact maps were computed to define predominant C99−Chol contacts at contact interfaces stabilized for various chemical states of C99 at 20 mol % Chol.

At interface 1 (Figure 9), which includes the GxxxG face, E22,D23[0], E22Q[0], and D23N[0] exhibit rare contacts to the C99 TMD and prominently feature H-bonds of Chol oxygen with K16 (occasionally with K28). These contacts were observed when the JM domain was positioned over the GxxxG face. While the population of interface 1 is higher than all other binding interfaces (Figure 8), C99−Chol complexes were not observed to be stabilized by contacts with the GxxxG face in conjunction with the JM domain as originally hypothesized by Beel et al.[27] The GxxxG face only supports C99−Chol complexation when the JM domain is extended into solvent, as
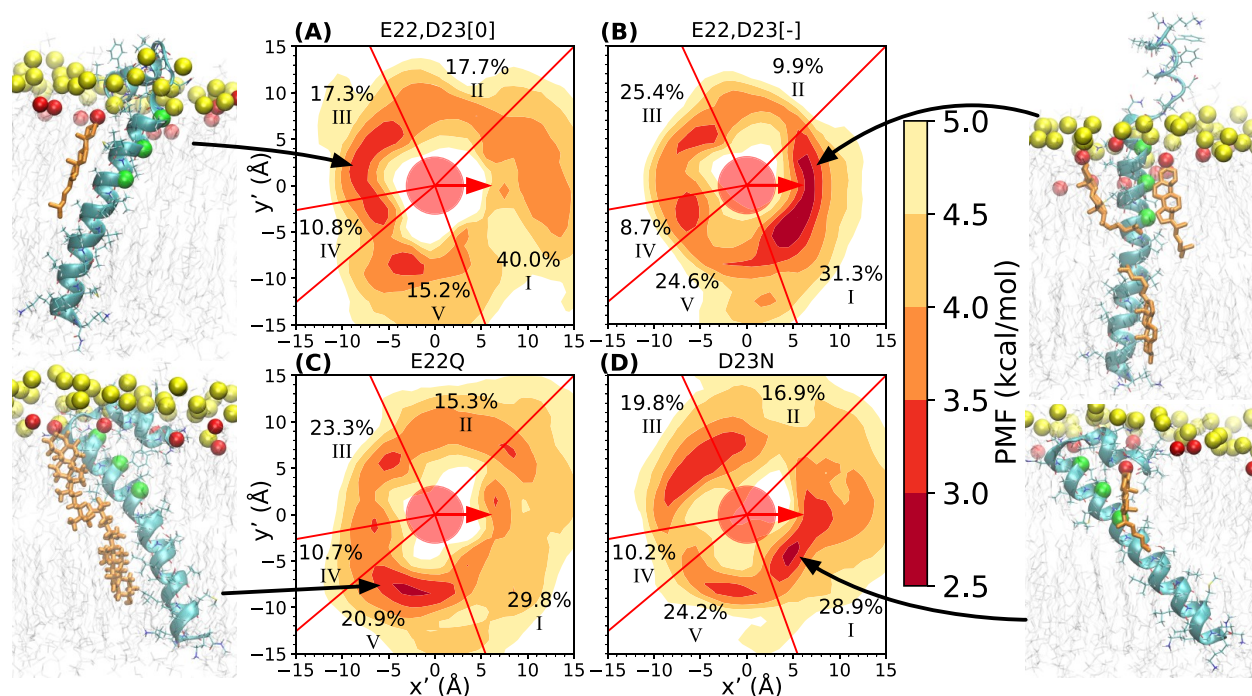
Figure 8. Potential of mean force ($-k_B T \ln p(x',y')$) about the GxxxG director vector (red) of the C99 TMD (circle). Five angular bins defining interfaces for upper leaflet TMD−Chol solvation demarcated by red lines. Insets display relative population of Chol at each of the five interfaces. Visualizations of C99−Chol complexes demonstrate representative configurations, depicting Chol (orange), $G_{29,33,37}$ (green), and DMPC and Chol phosphorus (yellow) and oxygen (red).

observed for E22,D23[−]. The complex is primarily stabilized by H-bonds of K28 with Chol O3 and π-stacking with ring B. Similarly, at other solvation interfaces where H-bonding with K28 to Chol O3 was observed, C99−Chol contacts were formed most prominently with the α-face of Chol with support from π-stacking with ring B and less frequently with the β-face, with Chol tail groups T_1 and T_2 contacting G38 and I41 (or G37 and V40) and A42 and I45 (or I41 and V44), respectively. C99 E22Q[0] and D23N[0] generally exhibit fewer contacts between the C99 TMD and sterol and tail groups of Chol.

At interface 2 (Figure 9), C99−Chol contacts were predominantly stabilized by hydrogen bonds with K16 in C99 E22,D23[0] and N27 and K28 in E22,D23[−] and E22Q[0]. D23N exhibits variable H-bonding of Chol with the JM domain in addition to N27 and K28. At interface 3, K28 H-bonding supports all observed C99−Chol contacts. In C99 E22,D23[−] and D23N[0], these contacts were also supported by K16 H-bonding. At interface 4, C99 E22,D23[0] exhibited prominent β-face binding chiefly stabilized via interaction of T_1 with G38 as well as I41 and T_2 with A42 and V45. C99 E22,D23[−] displayed solvation by the Chol α-face stabilized by various H-bonds with residues 27−30 and π-stacking with ring B. C99 E22Q[0] was observed to form occasional H-bonds solely with K28, while E22,D23[−], E22Q[0], and D23N[0] occasionally engaged in π-stacking with ring B. At interface 5, nonspecific H-bonds formed to the JM domain and turn region in E22,D23[0], accompanied by contacts of Chol tail groups with residues 40, 41, 44, and 45. E22,D23[−] and D22Q[0] both presented qualitatively similar contacts to those observed at interface 4. D23N[0] displayed prominent α- and β-face solvation stabilized by H-bonding with residues 26−30, most often with K28. For C99 E22,D23[−], H-bonding of the JM domain with Chol O3 occurred in the rare instances where

the unstructured JM domain was inserted in the membrane, as it was observed at interface 1.

Considering the C99−Chol interaction in the lower leaflet, absent a reentrant JM helix (including the C-helix[60]), Chol freely contacts residues at the C-terminal end of the TMD. We observed no specific interfaces for C99−Chol association along the C-terminal TMD of C99. Within the lower leaflet, E22,D23[0], E22,D23[−], and E22Q[0] were all observed to support C99−Chol association via H-bonding of Chol O3 to the lysine anchor $K_{53}K_{54}K_{55}$ and contact between the Chol β- and α-faces (via ring A) along the C-terminal end of the TMD (Figure S4). The end of the Chol tail (T_1, T_2) also forms many contacts with the TMD. D23N[0] Chol complexation in particular was found to be stabilized by interaction of L34 with T_2, facilitated by the enhanced tilt angle of the TMD (see Figure 3).

C99−DMPC Complex Solvates C99 without Specificity and Outcompetes Lys−Cholesterol Hydrogen Bonding. Given the pattern of C99−Chol solvation interfaces in the upper leaflet, it is reasonable to ask if solvating DMPC is characterized by a spatially complementary mass distribution about the C99 TMD. In fact, we find that C99−DMPC mass densities about the GxxxG face show virtually no preference of DMPC for any face of the C99 TMD (Figure 10). This further supports the conjecture that though cholesterol does not bind C99, it shows spatially anisotropic solvation of C99 (Figure 8), in contrast to lipids such as DMPC.

Analysis of C99−DMPC contact maps for dimer associations having >25 ns residence times reveal that, much like Chol, DMPC prominently interacts with the JM domain and the N-loop in addition to the TMD and the Lys anchor. However, interaction with Lys does not appear to be very important for stabilizing C99−DMPC complexes. This lack of specific interaction with Lys, which is responsible for
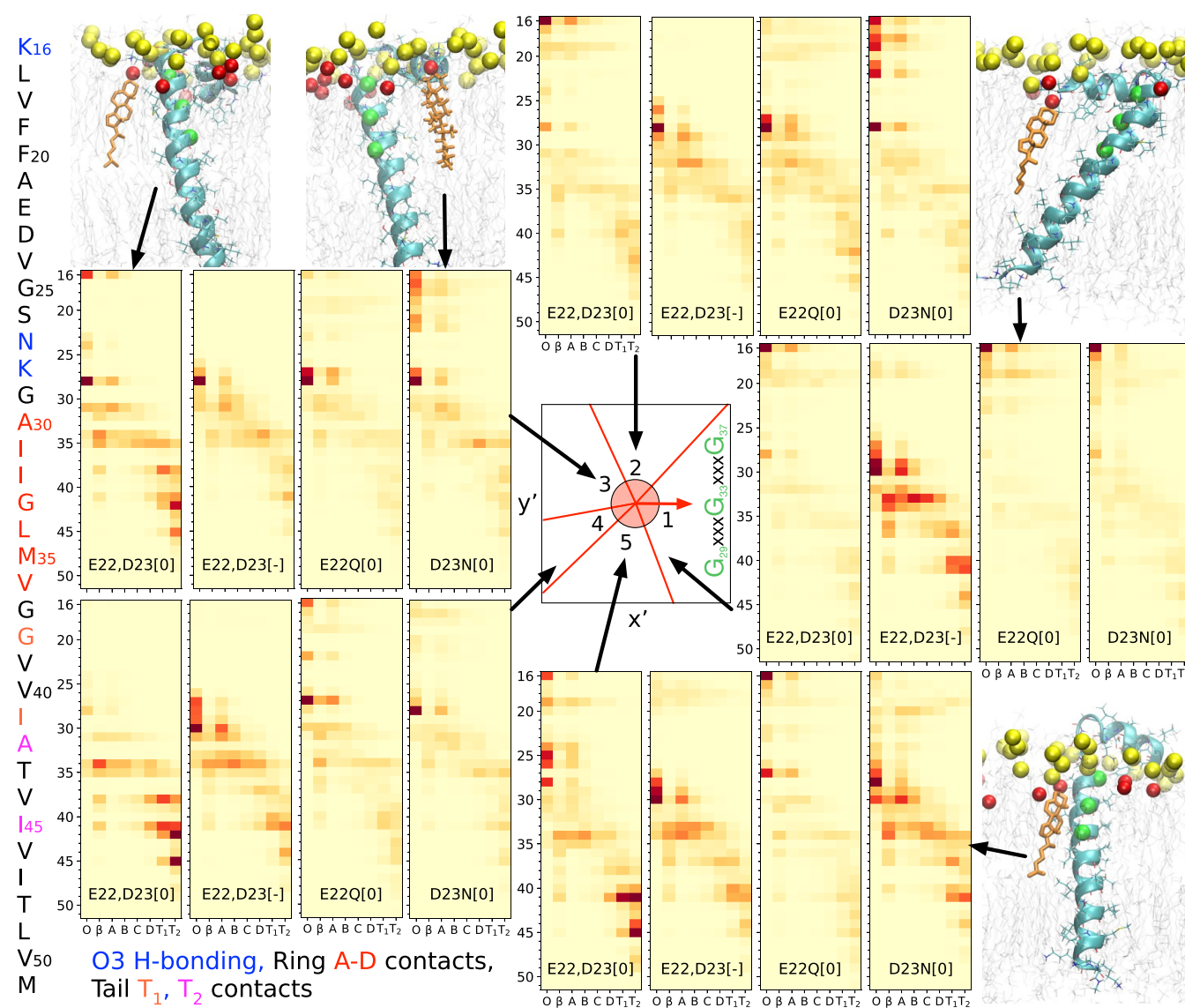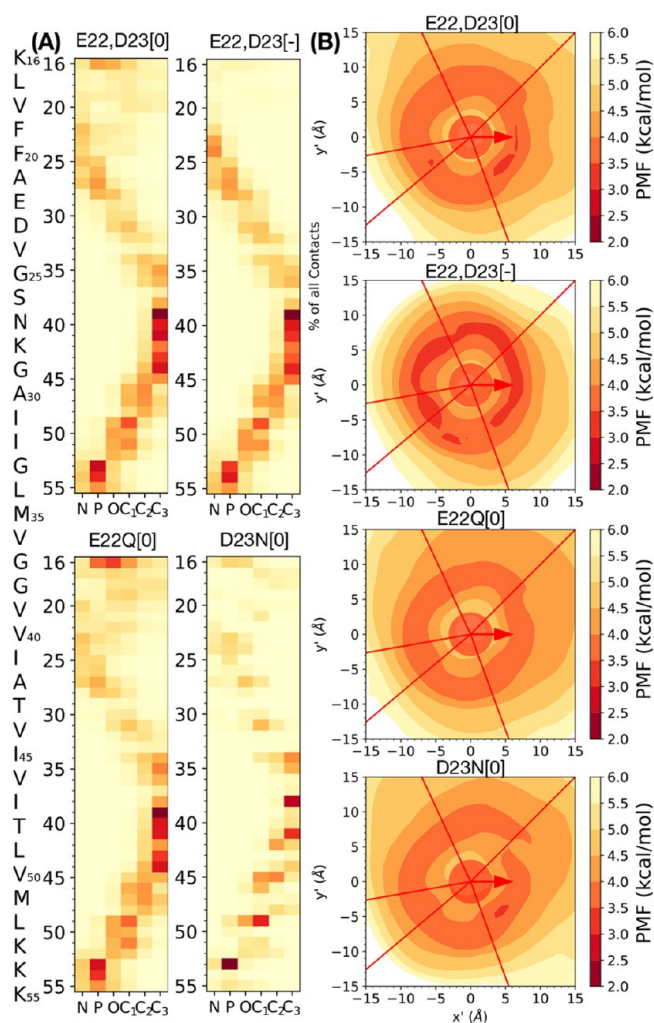
Figure 9. The >25 ns C99−Chol contact maps at 20 mol % for five upper leaflet C99−Chol solvation interfaces and four forms of C99. Populations are depicted in transformed *xy*-positions about the GxxxG face director vector (red arrow). Sampled contact likelihoods colored by relative position on a linear scale. Visualizations of representative C99−Chol complexes depicting Chol (orange), $G_{29,33,37}$ (green), and DMPC and Chol phosphorus (yellow) and oxygen (red).

dependence of Chol position on the orientation of the JM domain and N-loop, results in DMPC solvating the C99 TMD without orientational specificity.

We evaluate the average number of monopartite hydrogen bonds and salt bridges formed in each trajectory between one C99 and one Chol or DMPC averaged over the number of replicate trajectories (Table S3). The DMPC PC and ester groups each have four oxygens which form 44 potential monopartite hydrogen bonds or salt bridges with the five Lys of C99. The Chol hydroxyl group can form 17 monopartite hydrogen bonds with the Lys of C99. We observe that the Lys−PC salt bridge substantially outcompetes hydrogen-bonding groups, forming 6.7 times more often than the ester group and 53 times more often than the Chol hydroxyl group. This comparison does not account for the ratio of DMPC/Chol in these systems or the total number of potential monopartite hydrogen bonds available to the PC and ester groups compared to the hydroxyl group. Reweighting the average

number of Chol hydrogen bonds observed based on the DMPC/Chol (5/1 at 20 mol %) and the ratio of PC/hydroxyl (or ester/hydroxyl) potential hydrogen bonds and salt bridges (44/17), we find that the PC group is 4 times more likely to form a salt bridge with Lys than form a hydrogen bond with the Chol hydroxyl. However, we do find that the Chol hydroxyl is 1.7 times more likely to hydrogen bond with Lys than the DMPC ester if reweighted in this way. Perhaps it is this slightly higher affinity for the Chol hydroxyl group to Lys over the ester group that manifests this anisotropy around the TMD.

Recently, it was demonstrated that the phosphate−Lys interaction is 0.7 kcal/mol more stable than expected. It was suggested that the discrepancy could be corrected by increasing the minimum in the Lennard-Jones potential by 0.08 Å.[76] We did not employ this correction. However, it should be expected that interactions with PC and the hydrogen-bonding groups of sphingolipids and gangliosides

Figure 10. (A) The >25 ns C99−DMPC contact maps at 20 mol % Chol of both the upper and lower leaflet. (B) Potential of mean force ($-k_{B}T \ln p(x',y')$) of solvating DMPC about the GxxxG director vector (red) of the C99 TMD (circle) and red lines demarcating each of five C99−Chol interfaces.

that are found in lipid rafts, where C99 is evidenced to be processed, would outcompete Chol hydroxyl−Lys interactions. Within plasma membranes, where C99 is thought to play an important role in cholesterol homeostasis, the exo-facing leaflet generally has twice the saturated/unsaturated lipid ratio of the cyto-facing leaflet,[77] making it more likely that the N-terminus of C99, which forms specific but weak complexes with Chol, to be present in lipid raft domains. Therefore, though interactions that might contribute to stabilization of a specific, bound C99−Chol dimers are surpassed by interactions between other lipids in the membrane. Nevertheless, cholesterol is expected to interact with C99 in plasma membranes and affect its conformational ensemble.

■ SUMMARY AND CONCLUSIONS

Elucidation of the structure, stability, and possible function of C99−cholesterol complexation has received considerable attention since the initial report of specific binding of cholesterol to C99.[26,27] Functional roles proposed for specific binding of cholesterol to C99 have included cholesterol sensing, competition with C99 homodimerization, and C99 partitioning to L_o "raft" domains containing γ-secretase

involved in cleavage of C99 and Aβ biogenesis. Nevertheless, clear characterization of the structure of the C99−Chol complex has proved elusive. To address this fundamental question, we have employed unbiased, rigorously sampled atomistic molecular dynamics simulations to characterize the nature of C99−cholesterol interaction.

MD simulations of the wild-type sequence of the C99$_{16-55}$ congener protein were performed in DMPC lipid bilayers at 0, 5, 10, and 20 mol % concentrations, mimicking prior experimental studies of C99 in bicelles.[28] Formation of the L_o phase was observed at 20 mol % cholesterol, leading to an increase in tilt angle of C99 and impacting the depth of insertion of the JM domain and its orientation relative to the TMD. These changes may be indirectly responsible for changes in chemical shift initially attributed to the binding of cholesterol to C99[28] used to indirectly determine the equilibrium constant of C99−cholesterol dissociation.[32] Indeed, it was found that the C99 heterodimer lifetimes with cholesterol and DMPC manifest as similar power law distributions, displaying no clear signature of a bound C99−cholesterol heterodimer with a characteristic time scale and binding free energy.

For the purpose of investigating how complexed cholesterol might yet affect C99 structure, we investigated cholesterol and DMPC with C99 heterodimer lifetimes exceeding 25 ns as representative of long-lived complexes. We characterized the structure of C99 and C99−cholesterol interactions for C99 charged states representative of endosomal membranes at pH ≤ 6.5 (E22,D23[0]) and plasma membranes at neutral pH (E22,D23[−]) as well as the Dutch (E22Q[0]) and Iowa (D23N[0]) FAD mutants at pH ≤ 6.5. At 20 mol % cholesterol we found the C99 E22,D23[−] JM domain α-helix to be unstructured and extended into aqueous solvent. In contrast, in E22,D23[0], E22Q[0], and D23N[0] the JM domain features a structured α-helix. Of these, E22,D23[0] and D23N[0] were able to "switch" between a membrane-inserted and membrane-evacuated structure, while E22Q[0] was found to be exclusively inserted into the lipid bilayer.

The wild-type sequence of C99 was observed to support many different orientations of the JM domain relative to the GxxxG face, supporting multiple interfaces for solvation by cholesterol. E22Q[0] and D23N[0] do not exhibit pH switching behavior, instead consistently presenting a stable JM domain α-helix and a restricted set of conformational states. In the upper leaflet, five interfaces defined by orientation of Chol density relative to the GxxxG face were found to describe conformations of the C99 TMD solvated by cholesterol, having free energies derived from potential of mean force calculations within 1 kcal/mol of the experimentally derived dissociation constant.[32] Most complexes were stabilized by H-bonding of the cholesterol hydroxyl group to K16 and K28 and π-stacking interaction of the second cholesterol ring with the C99 TMD. Within the lower leaflet, complexes were characterized by H-bonding of cholesterol to the lysine anchor $K_{53}K_{54}K_{55}$, nonspecific contacts along the α- and β-face of cholesterol, and interaction of the cholesterol tail with the center of the C99 TMD.

Curiously, it was found that C99−DMPC complexes did not exhibit the specificity for interfaces on the C99 TMD as observed for cholesterol. We attribute this to the lack of necessity for specific interactions with Lys to stabilize the complex as is observed with C99−Chol. Additionally, it was found that DMPC outcompetes cholesterol for hydrogen

bonding with Lys, even when weighted for the total number of monopartite hydrogen bonds and salt bridges that may be formed and the DMPC/cholesterol ratio. This further supports the notion that cholesterol does not bind to C99, as the necessary hydrogen bonds are quickly replaced by competition with strongly interacting groups from other lipids.

Using unbiased MD simulations of C99 in DMPC−cholesterol lipid bilayers, we have provided insight into the atomic-level details of C99−cholesterol interactions. Our work suggests that there is no specific C99−cholesterol dimerization interface as initially hypothesized by Beel et al.[26] and that the large C99−Chol dissociation constant determined by Song et al.[32] is consistent with short-lived but specific C99−cholesterol complexes observed in our simulations. Recently proposed[42] roles for C99 regulation of cholesterol homeostasis and Aβ production suggest a role for both lipid raft domains and the pH cellular compartments. The multiple weak cholesterol solvation interfaces with C99 that we describe in this work provide insight into C99−Chol interactions that may play a key role in those environments.

■ ASSOCIATED CONTENT

SI Supporting Information

The Supporting Information is available free of charge at https://pubs.acs.org/doi/10.1021/acs.jpcb.0c07615.

> Populations of states in angle of JM domain to GxxxG face at 20 mol %; average lifetimes of C99−Chol encounter complexes; average and weighted number of Lys hydrogen bonds; carbon−deuterium order parameters of DMPC; C99−Chol residence times at 5−20 mol % Chol; number of concurrently solvating Chol to C99; C99−Chol contact maps at 20 mol % in lower leaflet (PDF)

■ AUTHOR INFORMATION

Corresponding Author

John E. Straub − *Department of Chemistry, Boston University, Boston, Massachusetts 02215, United States;* ◉ orcid.org/0000-0002-2355-3316; Email: straub@bu.edu

Authors

George A. Pantelopulos − *Department of Chemistry, Boston University, Boston, Massachusetts 02215, United States*

Afra Panahi − *Department of Chemistry, Boston University, Boston, Massachusetts 02215, United States*

Complete contact information is available at:
https://pubs.acs.org/10.1021/acs.jpcb.0c07615

Notes

The authors declare no competing financial interest.

■ ACKNOWLEDGMENTS

■ REFERENCES

(1) Simons, M.; Keller, P.; De Strooper, B.; Beyreuther, K.; Dotti, C. G.; Simons, K. Cholesterol depletion inhibits the generation of beta-amyloid in hippocampal neurons. *Proc. Natl. Acad. Sci. U. S. A.* **1998**, *95*, 6460−6464.

(2) Refolo, L. M.; Pappolla, M. A.; Malester, B.; LaFrancois, J.; Bryant-Thomas, T.; Wang, R.; Tint, G. S.; Sambamurti, K.; Duff, K. Hypercholesterolemia accelerates the Alzheimer's amyloid pathology in a transgenic mouse model. *Neurobiol. Dis.* **2000**, *7*, 321−331.

(3) Refolo, L. M.; Pappolla, M. A.; LaFrancois, J.; Malester, B.; Schmidt, S. D.; Thomas-Bryant, T.; Tint, G. S.; Wang, R.; Mercken, M.; Petanceska, S. S.; et al. A cholesterol-lowering drug reduces β-amyloid pathology in a transgenic mouse model of Alzheimer's disease. *Neurobiol. Dis.* **2001**, *8*, 890−899.

(4) Shie, F.-S.; Jin, L.-W.; Cook, D. G.; Leverenz, J. B.; LeBoeuf, R. C. Diet-induced hypercholesterolemia enhances brain Aβ accumulation in transgenic mice. *NeuroReport* **2002**, *13*, 455−459.

(5) Puglielli, L.; Tanzi, R. E.; Kovacs, D. M. Alzheimer's disease: the cholesterol connection. *Nat. Neurosci.* **2003**, *6*, 345−351.

(6) Zinser, E. G.; Hartmann, T.; Grimm, M. O. Amyloid beta-protein and lipid metabolism. *Biochim. Biophys. Acta, Biomembr.* **2007**, *1768*, 1991−2001.

(7) Yan, J.; Xu, Y.; Zhu, C.; Zhang, L.; Wu, A.; Yang, Y.; Xiong, Z.; Deng, C.; Huang, X. F.; Yenari, M. A. Simvastatin prevents dopaminergic neurodegeneration in experimental parkinsonian models: The association with anti-inflammatory responses. *PLoS One* **2011**, *6*, e20945.

(8) Wood, W. G.; Li, L.; Muller, W. E.; Eckert, G. P. Cholesterol as a causative agent in Alzheimer disease: a debatable hypothesis. *J. Neurochem.* **2014**, *129*, 559−572.

(9) Marquer, C.; Devauges, V.; Cossec, J.-C.; Liot, G.; Lécart, S.; Saudou, F.; Duyckaerts, C.; Lévêque-Fort, S.; Potier, M.-C. Local cholesterol increase triggers amyloid precursor protein-Bace1 clustering in lipid rafts and rapid endocytosis. *FASEB J.* **2011**, *25*, 1295−1305.

(10) Sengupta, U.; Nilson, A. N.; Kayed, R. The Role of Amyloid-β Oligomers in Toxicity, Propagation, and Immunotherapy. *EBioMedicine* **2016**, *6*, 42−49.

(11) Prasansuklab, A.; Tencomnao, T. Amyloidosis in Alzheimer's Disease: The Toxicity of Amyloid Beta (A β), Mechanisms of Its Accumulation and Implications of Medicinal Plants for Therapy. *Evidence-Based Complementary and Alternative Medicine* **2013**, *2013*, 1−10.

(12) Kayed, R. Common Structure of Soluble Amyloid Oligomers Implies Common Mechanism of Pathogenesis. *Science* **2003**, *300*, 486−489.

(13) Straub, J. E.; Thirumalai, D. Toward a molecular theory of early and late events in monomer to amyloid fibril formation. *Annu. Rev. Phys. Chem.* **2011**, *62*, 437−463.

(14) Steiner, H.; Fukumori, A.; Tagami, S.; Okochi, M. Making the final cut: pathogenic amyloid-β peptide generation by γ-secretase. *Cell Stress* **2018**, *2*, 292−310.

(15) Vetrivel, K. S.; Thinakaran, G. Membrane rafts in Alzheimer's disease beta-amyloid production. *Biochim. Biophys. Acta, Mol. Cell Biol. Lipids* **2010**, *1801*, 860−867.

(16) Hicks, D. A.; Nalivaeva, N. N.; Turner, A. J. Lipid Rafts and Alzheimer's Disease: Protein-Lipid Interactions and Perturbation of Signaling. *Front. Physiol.* **2012**, *3*, 1−18.

(17) Koo, E. H.; Squazzo, S. L. Evidence that production and release of amyloid β-protein involves the endocytic pathway. *J. Biol. Chem.* **1994**, *269*, 17386−17389.

(18) Wang, M.; Jing, T.; Wang, X.; Yao, D. Beta-secretase/BACE1 promotes APP endocytosis and processing in the endosomes and on cell membrane. *Neurosci. Lett.* **2018**, *685*, 63−67.

(19) Castro, M. A.; Hadziselimovic, A.; Sanders, C. R. The Vexing Complexity of the Amyloidogenic Pathway. *Protein Sci.* **2019**, pro.3606.

(20) Vist, M. R.; Davis, J. H. Phase equilibria of cholesterol/dipalmitoylphosphatidylcholine mixtures: 2H nuclear magnetic resonance and differential scanning calorimetry. *Biochemistry* **1990**, *29*, 451−464.

(21) Quinn, P. J.; Wolf, C. The liquid-ordered phase in membranes. Biochim. Biophys. Acta, Biomembr. 2009, 1788, 33−46.

(22) Sodt, A. J.; Sandar, M. L.; Gawrisch, K.; Pastor, R. W.; Lyman, E. The Molecular Structure of the Liquid-Ordered Phase of Lipid Bilayers. J. Am. Chem. Soc. 2014, 136, 725−732.

(23) Pantelopulos, G. A.; Straub, J. E. Regimes of Complex Lipid Bilayer Phases Induced by Cholesterol Concentration in MD Simulation. Biophys. J. 2018, 115, 2167−2178.

(24) Leeb, F.; Maibaum, L. Spatially Resolving the Condensing Effect of Cholesterol in Lipid Bilayers. Biophys. J. 2018, 115, 2179−2188.

(25) Kojro, E.; Gimpl, G.; Lammich, S.; Marz, W.; Fahrenholz, F. Low cholesterol stimulates the nonamyloidogenic pathway by its effect on the alpha-secretase ADAM 10. Proc. Natl. Acad. Sci. U. S. A. 2001, 98, 5815−5820.

(26) Beel, A. J.; Mobley, C. K.; Kim, H. J.; Tian, F.; Hadziselimovic, A.; Jap, B.; Prestegard, J. H.; Sanders, C. R. Structural Studies of the Transmembrane C-Terminal Domain of the Amyloid Precursor Protein (APP): Does APP Function as a Cholesterol Sensor? Biochemistry 2008, 47, 9428−9446.

(27) Beel, A. J.; Sakakura, M.; Barrett, P. J.; Sanders, C. R. Direct binding of cholesterol to the amyloid precursor protein: An important interaction in lipid-Alzheimer's disease relationships? Biochim. Biophys. Acta, Mol. Cell Biol. Lipids 2010, 1801, 975−982.

(28) Barrett, P. J.; Song, Y.; Van Horn, W. D.; Hustedt, E. J.; Schafer, J. M.; Hadziselimovic, A.; Beel, A. J.; Sanders, C. R. The Amyloid Precursor Protein Has a Flexible Transmembrane Domain and Binds Cholesterol. Science 2012, 336, 1168−1171.

(29) Javadpour, M. M.; Eilers, M.; Groesbeek, M.; Smith, S. O. Helix packing in polytopic membrane proteins: Role of glycine in transmembrane helix association. Biophys. J. 1999, 77, 1609−1618.

(30) Miyashita, N.; Straub, J. E.; Thirumalai, D.; Sugita, Y. Transmembrane structures of amyloid precursor protein dimer predicted by replica-exchange molecular dynamics simulations. J. Am. Chem. Soc. 2009, 131, 3438−3439.

(31) Dominguez, L.; Foster, L.; Straub, J. E.; Thirumalai, D. Impact of membrane lipid composition on the structure and stability of the transmembrane domain of amyloid precursor protein. Proc. Natl. Acad. Sci. U. S. A. 2016, 113, E5281−E5287.

(32) Song, Y.; Hustedt, E. J.; Brandon, S.; Sanders, C. R. Competition Between Homodimerization and Cholesterol Binding to the C99 Domain of the Amyloid Precursor Protein. Biochemistry 2013, 52, 5051−5064.

(33) Feldblum, E. S.; Arkin, I. T. Strength of a bifurcated H bond. Proc. Natl. Acad. Sci. U. S. A. 2014, 111, 4085−4090.

(34) Moore, D. T.; Berger, B. W.; DeGrado, W. F. Protein-Protein Interactions in the Membrane: Sequence, Structural, and Biological Motifs. Structure 2008, 16, 991−1001.

(35) Mueller, B. K.; Subramaniam, S.; Senes, A. A frequent, GxxxG-mediated, transmembrane association motif is optimized for the formation of interhelical C -H hydrogen bonds. Proc. Natl. Acad. Sci. U. S. A. 2014, 111, E888−E895.

(36) Anderson, S. M.; Mueller, B. K.; Lange, E. J.; Senes, A. Combination of $C\alpha$−H Hydrogen Bonds and van der Waals Packing Modulates the Stability of GxxxG-Mediated Dimers in Membranes. J. Am. Chem. Soc. 2017, 139, 15774−15783.

(37) Nierzwicki, Ł.; Czub, J. Specific binding of cholesterol to the amyloid precursor protein: Structure of the complex and driving forces characterized in molecular detail. J. Phys. Chem. Lett. 2015, 6, 784−790.

(38) Panahi, A.; Bandara, A.; Pantelopulos, G. A.; Dominguez, L.; Straub, J. E. Specific Binding of Cholesterol to C99 Domain of Amyloid Precursor Protein Depends Critically on Charge State of Protein. J. Phys. Chem. Lett. 2016, 7, 3535−3541.

(39) Benčina, M. Illumination of the spatial order of intracellular pH by genetically encoded pH-sensitive sensors. Sensors 2013, 13, 16736−16758.

(40) Levy, E.; Carman, M.; Fernandez-Madrid, I.; Power, M.; Lieberburg, I.; van Duinen, S.; Bots, G.; Luyendijk, W.; Frangione, B.

Mutation of the Alzheimer's disease amyloid gene in hereditary cerebral hemorrhage, Dutch type. Science 1990, 248, 1124−1126.

(41) Grabowski, T. J.; Cho, H. S.; Vonsattel, J. P. G.; Rebeck, G. W.; Greenberg, S. M. Novel amyloid precursor protein mutation in an Iowa family with dementia and severe cerebral amyloid angiopathy. Ann. Neurol. 2001, 49, 697−705.

(42) Montesinos, J.; Pera, M.; Larrea, D.; Guardia-laguarta, C.; Agrawal, R. R.; Velasco, K. R.; Yun, T. D.; Stavrovskaya, I. G.; Xu, Y.; Koo, S. Y.; et al. The Alzheimer's disease-associated C99 fragment of APP regulates cellular cholesterol trafficking. EMBO J. 2020, 39, 1−16.

(43) Levitan, I.; Singh, D. K.; Rosenhouse-Dantsker, A. Cholesterol binding to ion channels. Front. Physiol. 2014, 5, 1−14.

(44) Grouleff, J.; Irudayam, S. J.; Skeby, K. K.; Schiøtt, B. The influence of cholesterol on membrane protein structure, function, and dynamics studied by molecular dynamics simulations. Biochim. Biophys. Acta, Biomembr. 2015, 1848, 1783−1795.

(45) Sengupta, D.; Chattopadhyay, A. Molecular dynamics simulations of GPCR-cholesterol interaction: An emerging paradigm. Biochim. Biophys. Acta, Biomembr. 2015, 1848, 1775−1782.

(46) Hedger, G.; Sansom, M. S. Lipid interaction sites on channels, transporters and receptors: Recent insights from molecular dynamics simulations. Biochim. Biophys. Acta, Biomembr. 2016, 1858, 2390−2400.

(47) Fantini, J.; Di Scala, C.; Evans, L. S.; Williamson, P. T.; Barrantes, F. J. A mirror code for protein-cholesterol interactions in the two leaflets of biological membranes. Sci. Rep. 2016, 6, 21907.

(48) Genheden, S.; Essex, J. W.; Lee, A. G. G protein coupled receptor interactions with cholesterol deep in the membrane. Biochim. Biophys. Acta, Biomembr. 2017, 1859, 268−281.

(49) Rouviere, E.; Arnarez, C.; Yang, L.; Lyman, E. Identification of Two New Cholesterol Interaction Sites on the A2A Adenosine Receptor. Biophys. J. 2017, 113, 2415−2424.

(50) Barbera, N.; Ayee, M. A.; Akpa, B. S.; Levitan, I. Molecular Dynamics Simulations of Kir2.2 Interactions with an Ensemble of Cholesterol Molecules. Biophys. J. 2018, 115, 1264−1280.

(51) Song, W.; Yen, H. Y.; Robinson, C. V.; Sansom, M. S. State-dependent Lipid Interactions with the A2a Receptor Revealed by MD Simulations Using In Vivo-Mimetic Membranes. Structure 2019, 27, 392−403.

(52) Hedger, G.; Koldsø, H.; Chavent, M.; Siebold, C.; Rohatgi, R.; Sansom, M. S. Cholesterol Interaction Sites on the Transmembrane Domain of the Hedgehog Signal Transducer and Class F G Protein-Coupled Receptor Smoothened. Structure 2019, 27, 549−559.

(53) Fatakia, S. N.; Sarkar, P.; Chattopadhyay, A. A Collage of Cholesterol Interaction Motifs in the Serotonin1A Receptor: An Evolutionary Implication for Differential Cholesterol Interaction. Chem. Phys. Lipids 2019, 221, 184−192.

(54) Lee, A. G. Interfacial binding sites for cholesterol on G protein coupled receptors. Biophys. J. 2019, 116, 1586.

(55) Li, H.; Papadopoulos, V. Peripheral-type benzodiazepine receptor function in cholesterol transport. Identification of a putative cholesterol recognition/interaction amino acid sequence and consensus pattern. Endocrinology 1998, 139, 4991−4997.

(56) Fantini, J.; Barrantes, F. J. How cholesterol interacts with membrane proteins: an exploration of cholesterol-binding sites including CRAC, CARC, and tilted domains. Front. Physiol. 2013, 4, 1−9.

(57) Baier, C. J.; Fantini, J.; Barrantes, F. J. Disclosure of cholesterol recognition motifs in transmembrane domains of the human nicotinic acetylcholine receptor. Sci. Rep. 2011, 1, 69.

(58) Song, Y.; Mittendorf, K. F.; Lu, Z.; Sanders, C. R. Impact of Bilayer Lipid Composition on the Structure and Topology of the Transmembrane Amyloid Precursor C99 Protein. J. Am. Chem. Soc. 2014, 136, 4093−4096.

(59) Massi, F.; Peng, J. W.; Lee, J. P.; Straub, J. E. Simulation study of the structure and dynamics of the Alzheimer's amyloid peptide congener in solution. Biophys. J. 2001, 80, 31−44.

(60) Pantelopulos, G. A.; Straub, J. E.; Thirumalai, D.; Sugita, Y. Structure of APP-C99 1−99 and implications for role of extra-membrane domains in function and oligomerization. *Biochim. Biophys. Acta, Biomembr.* **2018**, *1860*, 1698−1708.

(61) Pester, O.; Barrett, P. J.; Hornburg, D.; Hornburg, P.; Pröbstle, R.; Widmaier, S.; Kutzner, C.; Dürrbaum, M.; Kapurniotu, A.; Sanders, C. R.; et al. The backbone dynamics of the amyloid precursor protein transmembrane helix provides a rationale for the sequential cleavage mechanism of gamma-secretase. *J. Am. Chem. Soc.* **2013**, *135*, 1317−1329.

(62) Best, R. B.; Zhu, X.; Shim, J.; Lopes, P. E.; Mittal, J.; Feig, M.; MacKerell, A. D. Optimization of the additive CHARMM all-atom protein force field targeting improved sampling of the backbone ϕ, ψ and side-chain $\chi1$ and $\chi2$ Dihedral Angles. *J. Chem. Theory Comput.* **2012**, *8*, 3257−3273.

(63) Klauda, J. B.; Venable, R. M.; Freites, J. A.; O'Connor, J. W.; Tobias, D. J.; Mondragon-Ramirez, C.; Vorobyov, I.; MacKerell, A. D.; Pastor, R. W. Update of the CHARMM All-Atom Additive Force Field for Lipids: Validation on Six Lipid Types. *J. Phys. Chem. B* **2010**, *114*, 7830−7843.

(64) Nadezhdin, K. D.; Bocharova, O. V.; Bocharov, E. V.; Arseniev, A. S. Dimeric structure of transmembrane domain of amyloid precursor protein in micellar environment. *FEBS Lett.* **2012**, *586*, 1687−1692.

(65) Jo, S.; Kim, T.; Im, W. Automated builder and database of protein/membrane complexes for molecular dynamics simulations. *PLoS One* **2007**, *2*, e880.

(66) Jo, S.; Kim, T.; Iyer, V. G.; Im, W. CHARMM-GUI: A web-based graphical user interface for CHARMM. *J. Comput. Chem.* **2008**, *29*, 1859−1865.

(67) Brooks, B. R.; Brooks, C. L.; Mackerell, A. D.; Nilsson, L.; Petrella, R. J.; Roux, B.; Won, Y.; Archontis, G.; Bartels, C.; Boresch, S.; et al. CHARMM: The biomolecular simulation program. *J. Comput. Chem.* **2009**, *30*, 1545−1614.

(68) Wu, E. L.; Cheng, X.; Jo, S.; Rui, H.; Song, K. C.; Dávila-Contreras, E. M.; Qi, Y.; Lee, J.; Monje-Galvan, V.; Venable, R. M. CHARMM-GUI membrane builder toward realistic biological membrane simulations. *J. Comput. Chem.* **2014**, DOI: 10.1002/jcc.23702.

(69) Lee, J.; Cheng, X.; Swails, J. M.; Yeom, M. S.; Eastman, P. K.; Lemkul, J. A.; Wei, S.; Buckner, J.; Jeong, J. C.; Qi, Y.; et al. CHARMM-GUI Input Generator for NAMD, GROMACS, AMBER, OpenMM, and CHARMM/OpenMM Simulations Using the CHARMM36 Additive Force Field. *J. Chem. Theory Comput.* **2016**, *12*, 405−413.

(70) Abraham, M. J.; Murtola, T.; Schulz, R.; Pall, S.; Smith, J. C.; Hess, B.; Lindahl, E. Gromacs: High performance molecular simulations through multi-level parallelism from laptops to super-computers. *SoftwareX* **2015**, *1−2*, 19−25.

(71) Miyamoto, S.; Kollman, P. A. Settle: An analytical version of the SHAKE and RATTLE algorithm for rigid water models. *J. Comput. Chem.* **1992**, *13*, 952−962.

(72) Di Pierro, M.; Elber, R.; Leimkuhler, B. A Stochastic Algorithm for the Isobaric−Isothermal Ensemble with Ewald Summations for All Long Range Forces. *J. Chem. Theory Comput.* **2015**, *11*, 5624−5637.

(73) Cheng, A.; Merz, K. M. Application of the Nosé-Hoover Chain Algorithm to the Study of Protein Dynamics. *J. Phys. Chem.* **1996**, *100*, 1927−1937.

(74) Parrinello, M.; Rahman, A. Polymorphic transitions in single crystals: A new molecular dynamics method. *J. Appl. Phys.* **1981**, *52*, 7182−7190.

(75) Bandara, A.; Panahi, A.; Pantelopulos, G. A.; Straub, J. E. Exploring the structure and stability of cholesterol dimer formation in multicomponent lipid bilayers. *J. Comput. Chem.* **2017**, *38*, 1479−1488.

(76) Yoo, J.; Aksimentiev, A. New tricks for old dogs: Improving the accuracy of biomolecular force fields by pair-specific corrections to non-bonded interactions. *Phys. Chem. Chem. Phys.* **2018**, *20*, 8432−8449.

(77) Lorent, J. H.; Levental, K. R.; Ganesan, L.; Rivera-Longsworth, G.; Sezgin, E.; Doktorova, M.; Lyman, E.; Levental, I. Plasma membranes are asymmetric in lipid unsaturation, packing and protein shape. *Nat. Chem. Biol.* **2020**, *16*, 644−652.